SCIENTIFIC Publishing Limited

Soil Health and Sustainability

https://ojs.ukscip.com/index.php/SHS

Article

Hybrid-Coupled Solution Model for the Internal Energy Equation: Hydrogeomechanics HGM

Eduardo Teófilo-Salvador

Division of Earth Sciences Engineering, Faculty of Engineering, National Autonomous University of Mexico, Mexico City 04510, Mexico; teofilo.salvador@ciencias.unam.mx

Received: 26 June 2025; **Revised:** 9 August 2025; **Accepted:** 12 September 2025; **Published:** 9 October 2025

Abstract: Water infiltration and recharge cause stresses, deformations, and displacements in the soil, which can lead to landslides, subsidence, erosion, etc. The objective was to propose a solution for the internal energy equation, (water flow in the soil mass) based on modern mechanics and underground hydraulics. From continuum mechanics, the internal energy equation was analyzed: i) the distribution of water flow at the surface as a source; ii) the expansion of water flow within the soil mass in cylindrical coordinates; iii) the distribution at the upper boundary, and the transient conduction of internal radial flow. Analogous near-surface and internal conduction were proposed as a load source. Stresses, deformations, displacements, and potentials were reviewed using modern mechanics, and the superposition principle was applied. The formulation was applied to a case study. It was found that Cartesian equations best represent the external surface flow of water (runoff), while cylindrical and radial equations best fit the internal flow in the soil (conduction-distribution). The proposed solution is in terms of the supplied load (precipitation). At different soil moisture contents—dry, saturated, and supersaturated—dynamic processes generate different energy rates. Externally, in supersaturated soils, the energy is purely hydraulic and is a parallel mobilization force on the surface (runoff or flooding). This solution could be applied to other multidisciplinary problems in mechanics, geomechanics, and hydrogeology, given the rigor of mathematical formulations that have described problems independently.

Keywords: Hydrogeomechanical Coupling; Thermal Analogy-Hydraulics; Hybrid/Coupled Flow Solution

1. Introduction

Hybrid systems need mathematical models that combine the dynamics of continuous parts, which consist of differential equations, and are important in multidisciplinary designs around us, according to Heemels et al. [1]. For example, Mittal et al. [2] proposed the development of superporous hybrid hydrogel compounds, with high water vapor adsorption capacity, associated with isotherms and adsorption kinetics. Tran et al. [3] proposed a hybrid discrete-continuous numerical framework, for the hydromechanical behavior of soil at granular, and macroscopic scales to predict desiccation cracking in clay soils. Pan et al. [4] proposed a hybrid analysis method for soil-water mass interaction, the solid phase (soil), whose movement is represented with a Lagrangian description, while the fluid phase (water), is adapted to the Eulerian description. El-Zorkany and Balasubramanian [5] presented the hybrid computer solution of the Laplace approximation modified by Galerkin, solving linear and nonlinear problems. Asaoka et al. [6] applied a coupled soil-water finite deformation analysis, using the Cam-Clay model with undrained triaxial compression testing, indicating that a single soil sample produces a highly heterogeneous state. Lima et al. [7] reviewed the hybrid numerical-analytical solution of the Navier-Stokes equations, Reynolds number

averaged for turbulent flow in parallel plates. Erduran [8] introduced the hybrid scheme for the solutions of the Boussinesq equations, composed of the finite volume method, and the finite difference method. While, Huang and Rudolph [9] presented a hybrid analytical-numerical scheme, for one-dimensional soil temperature profiles under freezing (or thawing) conditions, divided into multiple layers. Nastase [10] proposed hybrid solutions for compressed Navier-Stokes boundary layers, with external flow without parallel flow. Xie et al. [11] presented a semi-implicit method for modeling large deformations, with a semi-implicit approach that eliminates the dependence on the passage of time, in coupled soil-water problems. Chen [12] analyzed hyperbolic heat conduction problems in cylindrical coordinate systems using the hybrid Green's function method. Luo et al. [13] proposed a mathematical model of thermal-hydric-saline coupling for frozen unsaturated saline soils, considering phase change, impedance, consumption, and precipitation. Madureira and Melo [14] showed a method to evaluate the stress intensity in hydraulic cracks using a hybrid solution in pipes. Nick and Matthäi [15] demonstrated that the hybrid finite element, and finite volume method has great potential in realistic simulations of flow, and transport in heterogeneous porous media.

Zhang et al. [16] implemented a coupled numerical model that included water migration in the vapor and liquid phases, and heat transfer by conduction, which predominated in the deepest layer of soil (below 75 cm). Sun et al. [17] presented a new coupled radial-vertical filtration model within liquefiable soil, to determine the performance of stone column reinforcement, incorporating deformation and boundary conditions. Tu et al. [18] proposed a three-dimensional continuous-discrete method, the soil deformations were determined using the discrete element method, and the fluid flow in the soil phase was determined using the Darcy fluid and continuity equation. Hai et al. [19] applied Darcy's law, heat conduction, the solid-liquid relationship and relative saturation, and adjusted their soil-water characteristic curves to reflect the hydrothermal evolution of the soil. Deng et al. [20] indicate that the complex dynamics between plant-soil-water interactions can generate inaccuracies, due to the high complexity of using integrated models; they present a coupled model, DayCent-MODFLOW, for areas with shallow groundwater. Nguyen and Indraratna [21] mention that the filtration flow causes a reduction in the effective soil stress. Thus, they evaluate the evolution of energy in soil fluidization with discrete elements coupled, with computational fluid dynamics. Sun et al. [22] compared the effects of three depths on the coupling characteristics of the soil water-root system, finding that increasing the depth can cause water migration.

Wang et al. [23] propose a coupled continuous water-structure-saturated media model, to investigate the seismic response of the system under vertical seismic excitation. Shao et al. [24] mention that there are a few modeling, and coupling analysis studies to relate soil properties to production and yield, associating stability in the soil layer of 20 to 40 cm. As has been seen, water is the main driver, and it can dominate the coupling of systems, such as vegetation-soil systems, and soil nutrients, according to Han et al. [25], thereby affecting root growth, plant growth, or descent to deeper layers.

Hydrogeology, Geomechanics, and Internal Energy Equation

The surface flow must include topography, with discretized terms, verified and validated with experimentation either in the field, or laboratory with spatio-temporal discontinuities, indicated by Ambati and Bokhove [26]. For groundwater flow based on mathematical equations with assumptions and simplifications, as Atangana and Botha [27]. According to Raats and Gardner [28], cylindrical and radial flow systems require methods to determine the hydraulic conductivity of the soil as a function of the pressure head, so empirical functions such as the characteristic curve and the hydraulic conductivity function have been developed, described by López-Acosta [29].

In elasticity problems, the objective is to find the field of displacements and tensions in a homogeneous and isotropic body in a semi-infinite or infinite space, such as the Cerruti problem or that of Boussinesq, Flamant, Kelvin, Melan, and Mindlin, which have been very useful in Mechanics, Geotechnics, and Tribology, according to Nowinski [30], and Marmo et al. [31]. Li and Zou [32] analyzed two solutions to the problem of cavity expansion in drained and undrained conditions in soil mass, with analysis of large deformations. According to Ye et al. [33], various evolutionary systems are subject to rapid change, such as the variation of internal energy in a porous medium due to external and internal forces generated by the flow, indicated by Teófilo-Salvador et al. [34].

The energy equation describes the interaction of variables in Continuum Mechanics, Fluid Mechanics, and Modern Mechanics, and currently, no record has been found on the coupling of these disciplines to propose solutions to the internal energy equation. Furthermore, let it be a function of a single variable, for example, displacement as

a function of time, volume, and surface as functions of radius and weight, mentioned by Courant and John [35], but some hybrid or coupled models avoid solutions to discontinuous differential equations, so as not to solve non-linear problems, according to Sanfelice et al. [36]. Hybrid systems address particular, isolated, or specific problems, since conventional techniques or methodologies are still applied.

The problem of the soil mass water flow system consists of estimating a function in terms of a single variable, with direct dependence between the variables in different coordinate systems. Assuming analogy as a principle to develop solutions to problems that have been successfully applied in other areas or systems. The objective of the research was, to propose a solution for the internal energy equation (soil mass water flow) based on Modern Mechanics and Underground Hydraulics. With the transfer of flow from the surface to the interior of the porous medium, analyzing the stresses, deformations, and displacements based on a single variable. The principle is based on proposing an analogy between Darcy's law (fluid flow), and Fourier's law (heat conduction) to apply solutions to the phenomenological equations, that describe transport through a medium. Furthermore, both laws establish that a flow (of water or heat) is proportional to the gradient of a driving force (pressure or temperature).

2. Methodology

The solution approach is formulated with theoretical-mathematical bases, maturity is given by the approach itself, no development steps are omitted, and the formulation and coupling are shown. The foundations and premises are cited and serve to support the videos published by Teófilo-Salvador, on how the solution models are posed (see links https://www.youtube.com/watch?v=6KSPdGEDIwY&t=6s, https://www.youtube.com/watch?v=wEO-TBTd4PU&t=1759s, https://www.youtube.com/watch?v=7uy71Y-xzgc&t=8s, https://www.youtube.com/watch?v=7dz-a4R9M6Y).

The internal energy equation for the water flow system in the soil mass was evaluated as an HGM model by Teófilo-Salvador et al. [34], in Cartesian coordinates of the extensive form as:

$$\begin{aligned}\rho\frac{du}{dt} = &\left[\sigma_{11}\frac{\partial u_1}{\partial x_1} + \frac{\sigma_{12}}{2}\left(\frac{\partial u_1}{\partial x_2} + \frac{\partial u_2}{\partial x_1}\right) + \frac{\sigma_{13}}{2}\left(\frac{\partial u_1}{\partial x_3} + \frac{\partial u_3}{\partial x_1}\right)\right.\\ &+\frac{\sigma_{21}}{2}\left(\frac{\partial u_1}{\partial x_2} + \frac{\partial u_2}{\partial x_1}\right) + \sigma_{22}\frac{\partial u_2}{\partial x_2} + \frac{\sigma_{23}}{2}\left(\frac{\partial u_2}{\partial x_3} + \frac{\partial u_3}{\partial x_2}\right)\\ &\left.+\frac{\sigma_{31}}{2}\left(\frac{\partial u_1}{\partial x_3} + \frac{\partial u_3}{\partial x_1}\right) + \frac{\sigma_{32}}{2}\left(\frac{\partial u_2}{\partial x_3} + \frac{\partial u_3}{\partial x_2}\right) + \sigma_{33}\frac{\partial u_3}{\partial x_3}\right]\\ &-\left[\left(\frac{\partial q_1}{\partial x_1} + \frac{\partial q_2}{\partial x_2} + \frac{\partial q_3}{\partial x_3}\right)\right] + \rho P\end{aligned} \tag{1}$$

Where u was the internal energy, t the time, u deformation in direction x_i, i = 1, 2, 3, σ the stress, ρ the density, and P the source, that this case was the applied load.

2.1. Distribution of Source Flow Supply

It was considered: i) the presence of a first layer of soil with vegetation exposed to the atmosphere, with free flow of water from the source, ii) plant evapotranspiration tended to zero, compared to the hydraulic conductivity of the root zone. The system was assumed to be continuous, when considering Rakoto-Ravalontsalama [37], to establish conditions of stability and uniformity, according to Ye et al. [33]. Since the ordinary differential equations of the internal energy equation are associated with a dynamic system, with time, space, initial states, and movements, when considering Michel et al. [38]. It was assumed that at various points of the upper limit of the soil mass, the source distribution (raindrops) generated surface forces and that these were equivalent to a resultant force P, with local wetting bulbs (**Figure 1**).

With the uniform distribution of water over the upper limit, any point at a distance $2r$ from the point of application of the force was subject to axial compression in the radial direction, when r and d tended to zero, the resultant was a point in the surface space of the soil, and the distribution of particles p on the surface was associated with the point P. If the resultant sum of the forces p exerted at distances d on the surface was continuous and uniform, then the local distribution obeyed a resultant as:

$$P = \sum_{i=1}^{n} p_i + \Delta FS \tag{2}$$

From *i* to *n* accumulated raindrops, with subsurface water flow ΔFS, according to Teófilo-Salvador et al. [39]. For $r > 0$, where $0 \leq \theta \leq \pi$, and $0 \leq \phi \leq \alpha$, α was the angle of inclination of the soil surface, and z took any depth value. Given rainfall distributions with a beginning, peak, and decrease, formulations were investigated that would allow describing the probability distribution, similar to the Rayleigh distribution, and a gamma-type distribution (Erlang-2). Therefore, these distribution functions were proposed as analogous to a precipitation load function as a function of time $P(t)$, expressed as:

$$P(t) = \frac{t}{\omega} e^{-\frac{t^2}{2\omega}} \quad , \quad P(t) = \omega^2 t e^{-\omega t} \tag{3}$$

ω was a measure of the distribution of rain load over time *t*, for large and small values, respectively. Since, for long times, the distribution is smoother (flattened), and for short times they present a more pronounced peak, assuming interception, evaporation, and evapotranspiration are negligible, for large rainfall values. The interaction of these two expressions led to the proposal of the presence of oscillations during a rain event, on the surface, with a maximum and a minimum as a non-periodic simple harmonic variable pulse function in one dimension.

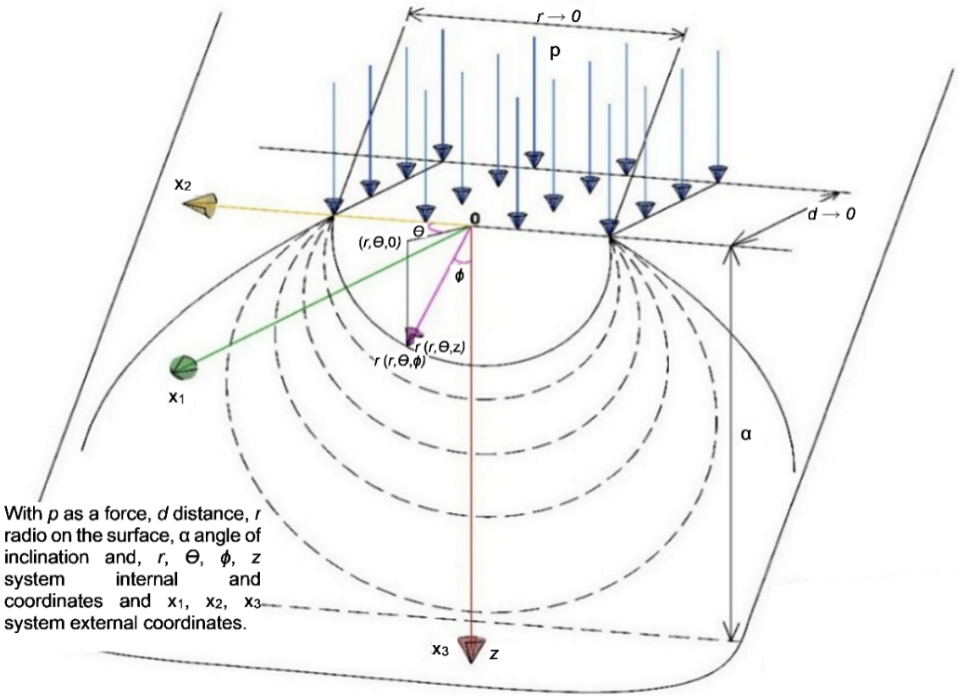

Figure 1. Coordinate systems with applied load *p* and internal bulbs in a porous medium.

2.2. Expansion of the Water Flow within the Soil Mass

Richards [40] and Richardson [41] developed a physical–mathematical model, an equation that combines mass conservation and Darcy-Buckingham flux relationship:

$$\frac{\partial \theta(\psi)}{\partial t} = \nabla \cdot [K(\psi) \nabla \psi] + \frac{\partial K(\theta)}{\partial z} \tag{4}$$

Where θ is the volumetric water content, ψ is the matric component of soil water potential per weight, $K(\psi)$ (or $K(\theta)$ in a different form) is the unsaturated hydraulic conductivity function, indicated by Xiong [42]. Thus, from the saturated transient flow equation in cylindrical coordinates:

$$\frac{\partial}{\partial r}\left(K_r \frac{\partial h}{\partial r}\right) + \frac{K_r}{r}\left(\frac{\partial h}{\partial r}\right) + \frac{1}{r^2}\frac{\partial}{\partial \theta}\left(K_\theta \frac{\partial h}{\partial \theta}\right) + \frac{\partial}{\partial z}\left(K_z \frac{\partial h}{\partial z}\right) = \frac{\partial h}{\partial t} \tag{5}$$

The hydraulic head *h* was a function of the position *z* without linearity in the groundwater flow equations. As the dependence and relationship of variables for the matrix potential of the moisture content, conductivity, and

hydraulic head did not allow obtaining an exact universal solution, mentioned by Philip [43], it was necessary to propose, in this research: i) surface conduction, ii) radial conduction of the flow, and iii) radial and axial distribution.

2.2.1. Distribution at the Upper Boundary

The soil evaporative layer was a limit to eventually avoid drastic soil-water changes, and the lower limit, the source flow did not return to the atmosphere. With initial moisture content, $K = K_0$ for a homogeneous and isotropic system, the equivalence of the hydraulic load h with the variations in the moisture content θ was assumed, the latter only depended on the position r, so the conduction of the flow oscillated at time t, with a source at velocity P_0, and in radial coordinates were:

$$\frac{\partial \theta}{\partial t} \equiv K_0 \frac{1}{r^2} \frac{\partial}{\partial r}\left(r^2 \frac{\partial \theta}{\partial r}\right) \equiv -P_0 \tag{6}$$

At constant hydraulic conductivity in time, it was possible to apply a general solution for radial flow according to Carslaw and Jaeger [44], of the form:

$$\theta = \frac{A}{r} + B \tag{7}$$

Where A and B were constants determined by the boundary conditions, and at the upper limit, the moisture content tended to zero, $r \to 0$.

2.2.2. Transient Conduction of Internal Radial Flow

Based on Unsworth and Duarte [45], an analogous procedure, but for transient water flux in the soil mass, the moisture content at any point was only a function of r and t (**Figure 2**), the first two terms of Equation (5) were related to a function of the form $V = r\theta$, and the transformation was:

$$\frac{\partial^2 V}{\partial r^2} = \frac{1}{K} \frac{\partial V}{\partial t} \tag{8}$$

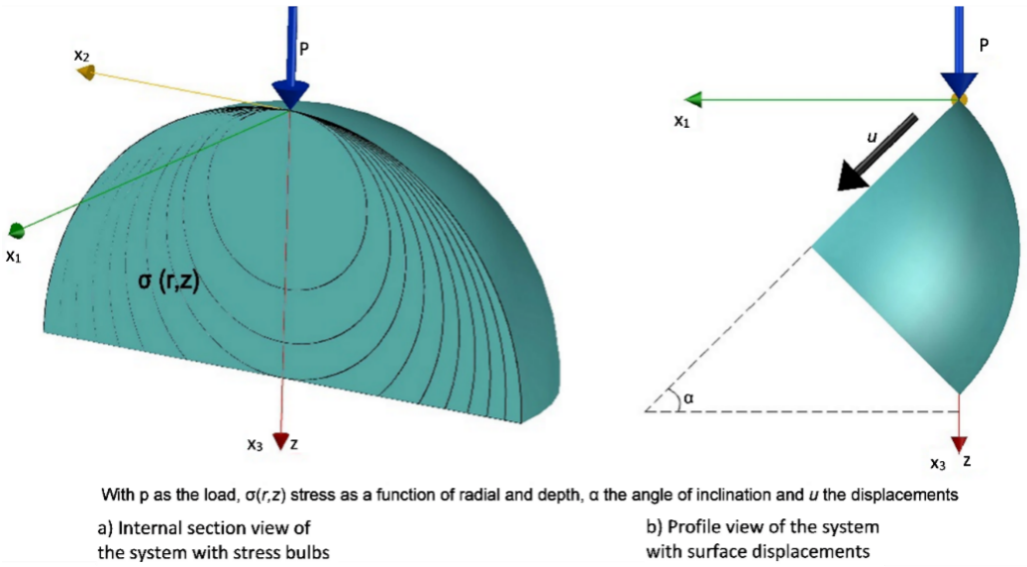

Figure 2. Vertical load applied to a porous medium, effects: (**a**) internal, (**b**) external.

A solution was proposed, and the method of separation of variables was applied:

$$V(r,t) = R(r)\theta(t) \tag{9}$$

$$\begin{aligned} \frac{\partial V}{\partial t} &= R(r)\theta'(t) \\ \frac{\partial^2 V}{\partial r^2} &= \theta(t)R''(r) \end{aligned} \tag{10}$$

The above was replaced in the initial approach, and we obtained:

$$\begin{matrix} R'' + \lambda^2 R = 0 \\ \theta' + K\lambda^2\theta = 0 \end{matrix} \quad (11)$$

For t = 0, then $\theta(t) = \theta(0)$, the previous expression was integrated, and obtained:

$$\theta(t) = \theta(0)e^{-K\lambda^2 t}$$

$$R = A\,cos\lambda r + B\,sin\lambda r \quad (12)$$

The composite solution to the problem posed was:

$$V(r,t) = \sum_{\lambda} (A\,cos\lambda r + B\,sin\lambda r)\,\theta(0)e^{-K\lambda^2 t} \quad (13)$$

For constants A and B, the flow behavior was defined in a volume (**Figure 2**) that was wetted or flooded at constant flow up to a moisture content θ_s. Subsequently, the source was removed, and the medium was exposed to ventilation or drying to a moisture content θ_r. The influence of drastic climatic conditions allowed us to assume that V = 0 at θ_r = 0, cyclically ($t_n = t_i$) when r = 0 and $r = \alpha$, at t = 0:

$$V_s = r\theta_s \quad (14)$$

When V = 0, r = 0, it implied that R = 0, but according to **Figure 1**, at $r = \alpha$

$$R = B\,sin\lambda r \quad (15)$$

It was evaluated A = 0

$$V(r,t) = \theta(0)\sum_{\lambda} B\,sin\lambda r e^{-K\lambda^2 t} \quad (16)$$

Applied sin$\lambda\alpha$ = 0, with $\lambda\alpha = n\pi$, in this way was expressed in:

$$V(r,t) = \theta(0)\sum_{n=1}^{\infty} B\,sin\frac{n\pi r}{a} exp\left(-Kt\frac{(n\pi)^2}{a^2}\right) \quad (17)$$

At t = 0, at the point (0, α), the constant B was determined as:

$$B = \frac{2}{a}\int_0^a r\,sin\frac{n\pi r}{a}dr = -\frac{2^{n+1}a}{n\pi} \quad (18)$$

2.2.3. Conduction Analogous to a Near-Surface Flow Supply Load

In **Figure 2**, the point-loaded solid of revolution was governed by:

$$R = \sqrt{x_1^2 + x_2^2 + x_3^2} \quad , \quad r = \sqrt{x_1^2 + x_2^2} \quad (19)$$

If the functions were continuous and the moisture distribution was a function of time, the solution to the flow equation had to satisfy the limit at all points in the solid. Based on Carslaw and Jaeger [44], and according to the characteristics of the three-dimensional flow equation, it was proposed:

$$\Theta = \frac{1}{8(\pi Kt)^{3/2}}\int_{-\infty}^{\infty}\int_{-\infty}^{\infty}\int_{-\infty}^{\infty} f(x_1,x_2,x_3)e^{-\left[\frac{x_1^2+x_2^2+x_3^2}{4Kt}\right]}dx_1dx_2dx_3 \quad (20)$$

For t > 0, at constant flow per unit volume per unit time in the region 0 < z < α, and the amount of flow at any point r, θ, z at time t, was expressed as:

$$\frac{Q_c r dr d\theta dz dt}{8(\pi Kt)^{\frac{3}{2}}} e^{-\left[\frac{R^2}{4Kt}\right]} \quad (21)$$

For constant water flow Q_c, the conduction velocity was given by:

$$Q_c = -4\pi r^2 K\frac{\partial\theta}{\partial r} = P \quad (22)$$

The limits of r in the z axis, with instantaneous distribution and at all points at constant flow, the radial component moved at constant speed.

2.3. Geomechanical Development

Once the water flow functions were defined, the stresses and displacements at all points within the volume of the soil mass were determined. The equations were expressed in terms of the stresses, since these are generated from and above the limit, and the displacements are the effect of the deformations. If the mass forces remained constant, the solution could be obtained by a biharmonic function. According to Slaughter [46], for conservative forces, it could be expressed in terms of a potential function, since any magnitude in any system was invariant.

a) Internal potentials due to load

The conduction of the flow in the soil mass changed the initial state, thereby expanding the volume, which was analogically related to the Helmholtz displacement potentials, and the stress, strain, and displacement relationships, to the deformation potential of Lame. In 1930, Garlekin demonstrated the shift in terms of second derivatives represented as a single vector function, including Poisson's ratio *v* and the Garlekin vector *V*, which was related to the Helmholtz potential. The Laplacian was developed for the radial, tangential, and axial components:

$$\nabla^2 V = \frac{\partial}{\partial r}\left(\frac{\partial V_z}{\partial r}\right) + \frac{1}{r}\frac{\partial V_z}{\partial r} + \frac{1}{r^2}\frac{\partial}{\partial \theta}\left(\frac{\partial V_z}{\partial \theta}\right) + \frac{\partial}{\partial z}\left(\frac{\partial V_z}{\partial z}\right) \tag{23}$$

To find the stress, strain, and displacement functions, the relationships with the Lame strain potential and the Garlekin vector of the shape were applied:

$$\begin{aligned} \sigma_r &= \frac{\partial}{\partial z}\left(v\nabla^2 V_z - \frac{\partial}{\partial r}\left(\frac{\partial V_z}{\partial r}\right)\right) \\ \sigma_\theta &= \frac{\partial}{\partial z}\left(v\nabla^2 V_z - \frac{1}{r}\frac{\partial V_z}{\partial r} - \frac{1}{r^2}\frac{\partial}{\partial \theta}\left(\frac{\partial V_z}{\partial \theta}\right)\right) \\ \sigma_z &= \frac{\partial}{\partial z}\left((2-v)\nabla^2 V_z - \frac{\partial}{\partial z}\left(\frac{\partial V_z}{\partial z}\right)\right) \end{aligned} \tag{24}$$

For the *z* component, the biharmonic condition was met in cylindrical coordinates, and the function was left in terms of $V = V_z e_z$, according by Sadd [47], and the displacements were estimated considering a *A* constant:

$$V_{x_1} = V_{x_2} = 0 \quad , \quad V_z = AR = A\sqrt{r^2 + z^2} \tag{25}$$

For displacements, the approach was:

$$\begin{aligned} 2\mu u_r &= -\frac{\partial^2 V_z}{\partial r \partial z} \\ 2\mu u_\theta &= -\frac{\partial^2 V_z}{\partial \theta \partial z} \\ 2\mu u_z &= 2(1-v)\nabla^2 V_z - \frac{\partial}{\partial z}\left(\frac{\partial V_z}{\partial z}\right) \end{aligned} \tag{26}$$

The Helmholtz potential with the Garlekin vector was given by:

$$\varphi = A\frac{(1-2v)}{2\mu}\left(\frac{z}{\sqrt{r^2+z^2}} + 0 + \frac{r}{\sqrt{r^2+z^2}}\right) = A\frac{(1-2v)}{2\mu}\frac{(z+r)}{R} \tag{27}$$

Differentiable components and second derivatives were obtained with respect to *r*, *θ,* and *z*. It was discretized and developed to obtain the displacement components according to the Lame potentials, and proposed a flow advance function:

$$\varphi = B\ log(R+z) \tag{28}$$

B was an arbitrary constant, again with differentiable components and second derivatives with respect to *r*, *θ*, and *z*. The superposition principle was applied for the Garlekin vector and the Lame potential in the z-axis and radial direction, respectively:

$$\sigma_z = -A\left[\frac{(1-2v)z}{R^3} + \frac{3z^3}{R^5}\right] - \frac{Bz}{R^5} \quad \wedge \quad 2\mu u_r = A\frac{rz}{R^3} + B\frac{r}{R(R+z)} \tag{29}$$

For the constants *A* and *B*, in cylindrical coordinates, the radius *r* goes from 0 to π and $z \to \alpha$, and the resultant of the forces exerted on the surface of radius *r* was equal to *P*, such that:

$$\int_0^a 2\pi R\sigma_z(r,a)dR + P = 0 \tag{30}$$

The integral was solved with a change of variables and initial and boundary conditions.

b) Surface potentials due to load

A similar procedure was carried out for the external surface force that acted parallel to the free surface (**Figure 2b**), with analogy to the Cerruti problem, in this case the direction of the force was parallel to the direction of the *x* axis, and the solution was obtained by combining a Garlekin vector and the Lame deformation potential, with the proposed vector components:

$$V_{x_1} = AR \quad , \quad V_{x_2} = 0 \quad , \quad V_{x_3} = Bx_1\, log\,(R + x_3) \tag{31}$$

$$\varphi = \frac{Cx_1}{R + x_3} \tag{32}$$

With the movement of the flow on the surface in Cartesian coordinates, the value of the constant C was determined.

2.4. Application Case

To apply the expressions to a real case, the data obtained by Teófilo-Salvador [48], since these studies make use of a multifunctional infiltrometer, which associates flow sheets (simulation of rainfall) as hydraulic loads on the soil, from this the relationship to three components of fluid flow mobilization in the porous medium: surface flow, lateral flow and vertical flow, in addition to this, the hydraulic conductivity, infiltration rate and base infiltration at various depths were obtained, including data from soil samples. The field values were: root zone thickness of the porous medium 42 cm, length in y = 80 cm, superficial length 100 cm, angle of inclination 28.61°, test time 2.32 h, hydraulic load 49.09 mm. Sampling values, porosity 11.69%, natural density 770 kg/m^3, moisture content 18 kg/kg, apparent density 650 kg/m^3, equivalent water layer of the root zone 49.09 mm (value hydraulic load). The values for the upper limit of the unsaturated zone were: porosity 38.95%, natural density 2,070 kg/m^3, relative volume of water 63.79%, apparent density 1,680 kg/m^3, equivalent water layer of the upper limit of the unsaturated zone 27.26 mm.

In Microsoft Excel 2019, data from experimental field tests were adjusted when null values were presented in the time period, and subsequently, the Kostiakov model was applied to smooth the behavior in the test periods for the hydraulic conductivity. For the imposed hydraulic load, the values of: ω = 0.1, 0.2, 0.5, 1, and 2 for 1.08 h (when the load stabilized or remained constant). P_o = 62.01 mm as the upper limit of the hydraulic load, for a volume of P_v = 55.46 m^3, P_r = 6.54 mm, theoretical values of θ = 10, θ_r = 5, θ_s = 100, and field θ_r = 18, with the purpose of comparing theoretical data with field data, for different residual moisture contents, while maintaining constant hydraulic conductivity K = 2.452 mm/h, v = 0.45, and μ =0.03. The values were graphed in several Excel sheets to describe the behavior of the functions described in this research work, noting the use of soil properties, field testing, cabinet adjustments, and finally the implementation of the solution equations to the coupled-hybrid hydrogeomechanical model.

3. Results

3.1. Surface Flow Load Supply Distribution Function

From the manipulation of variables for the load $P(t)$ as a function of time, the precipitation of n flow drops, we obtained:

$$P(t) = \omega t^2 e^{-2\omega t} \tag{33}$$

3.2. Water Flow Conduction in the Soil Mass

a) Distribution at the upper limit and internal conduction

The solutions if $r \to \alpha$, but α did not tend to infinity, were:

$$\theta = \frac{P_0}{6K}\left(\alpha^2 - r^2\right) \quad \wedge \quad \theta = \frac{P_0}{6hK}\left[h\left(a^2 - r^2\right) + 2a\right] \tag{34}$$

b) Transient conduction of the internal radial flow

According to Unsworth and Duarte [45], for this case, the solution was obtained:

$$V(r,t) = \theta(0)\sum_{n=1}^{\infty} \frac{2(-1)^{n+1}a}{n\pi}\, sin\frac{n\pi r}{a} exp\left(-Kt\frac{n^2\pi^2}{a^2}\right) \tag{35}$$

$$\theta(r,t) = \frac{2a}{r\pi}\theta(0)\sum_{n=1}^{\infty} \frac{(-1)^{n+1}}{n}\, sin\frac{n\pi r}{a} exp\left(-Kt\frac{n^2\pi^2}{a^2}\right) \tag{36}$$

When $r \to \alpha$, the moisture content was determined as:

$$\theta = \theta_{(0,t)} = 2\theta_s \sum_{n=1}^{\infty} (-1)^{n+1} exp\left(-Kt\frac{n^2\pi^2}{a^2}\right) \tag{37}$$

For the case in which $\theta_r \neq 0$, we obtained:

$$\frac{\theta - \theta_r}{\theta_s - \theta_r} = 2\sum_{n=1}^{\infty} (-1)^{n+1} exp\left(-Kt\frac{n^2\pi^2}{a^2}\right) \tag{38}$$

Mathematically, a solution has been obtained, where now the left-hand side can be equated to the empirical equation proposed by van Genuchten [49].

$$S_e = \frac{\theta - \theta_r}{\theta_s - \theta_r} = \frac{1}{\left[1 + (\alpha|h|)^n\right]^m} \tag{39}$$

Where S_e is the effective saturation, θ is the current volumetric moisture content, θ_r residual moisture content, θ_s is the moisture content at saturation, h pressure head (suction), and α, n, and m are empirical shape parameters.

c) Conduction analogous to a near-surface flow supply load

With initial moisture content θ_0, $r = 0$, $z = 0$, if the source distributions $P = Q_s = Q_c$ were continuous, uniform, and parallel to the axis z, without flow losses. It was then possible to estimate the moisture content at some time t. If $t \to \infty$ at steady state and with humidity at some point r, θ, z, the water flux solution was:

$$\Theta(r,z) = \frac{(P = Q_s = Q_c)}{4\pi K\,(r^2 + z^2)^{\frac{1}{2}}} e^{-\frac{\eta}{2K}\left[(r^2+z^2)^{\frac{1}{2}} - z\right]} \tag{40}$$

3.3. Distribution of Stresses, Deformations, and Displacements

a) Internal potentials due to charge

Consistent with Boussinesq's problem for a concentrated force perpendicular to the free surface, indicated by Sadd [47], the integration constants were:

$$A = \frac{P}{2\pi} \quad , \quad B = -\frac{(1-2v)P}{2\pi} \tag{41}$$

The tension components and the displacements as a function of the load P, were adequate compared with those estimated by the Papkovich method:

$$\begin{aligned} \sigma_r &= \frac{P}{2\pi}\left[\frac{(1-2v)}{R(R+z)} - \frac{3r^2z}{R^5}\right] \\ \sigma_\theta &= \frac{(1-2v)P}{2\pi}\left(\frac{z}{R^3} - \frac{1}{R(R+z)}\right) \\ \sigma_z &= -\frac{3P}{2\pi}\frac{z^3}{R^5} \end{aligned} \tag{42}$$

$$\begin{aligned} u_r &= \frac{P}{4\mu\pi}\left[\frac{rz}{R^3} - \frac{(1-2v)r}{R(R+z)}\right] \\ u_\theta &= 0 \\ u_z &= \frac{P}{4\mu\pi}\left[\frac{(2-2v)}{R} + \frac{z^2}{R^3}\right] \end{aligned} \tag{43}$$

b) Surface potentials due to the charge

Without radial symmetry, the integration constants in the x_1 and x_3 axes were:

$$A = \frac{P}{4\pi(1-v)} \quad , \quad B = \frac{(1-2v)P}{4\pi(1-v)} \quad , \quad C = \frac{(1-2v)P}{2\pi} \tag{44}$$

With a procedure similar to that of internal behavior, the stress functions as a function of the load *P*, for the external surface load, and the components of the resulting displacements, were consistent with the Cerruti problem:

$$\begin{gathered}\sigma_1 = \frac{P(1-2v)}{2\pi\ cos\alpha}\left[\frac{x_1}{R(R+x_3)^2} - \frac{2x_1x_2^2}{R^2(R+x_3)^3} - \frac{x_1x_2^2}{R^3(R+x_3)^2}\right] - \frac{3Px_1^2}{2\pi R^5} \\ \sigma_2 = \frac{P(1-2v)}{2\pi\ cos\alpha}\left[\frac{3x_1}{R(R+x_3)^2} - \frac{2x_1^3}{R^2(R+x_3)^3} - \frac{x_1}{R^3(R+x_3)^2}\right] - \frac{3Px_1x_2^2}{2\pi R^5} \\ \sigma_3 = \frac{3Px_1x_3^2}{2\pi R^5\ cos\alpha}\end{gathered} \tag{45}$$

$$\begin{gathered}u_1 = \frac{P}{4\pi\mu\ cos\alpha}\left[\frac{1}{R} + \frac{x_1^2}{R^3} + \frac{(1-2v)}{(R+x_3)} - \frac{x_1^2}{R(R+x_3)^2}\right] \\ u_2 = \frac{P}{4\pi\mu\ cos\alpha}\left[\frac{x_1x_2}{R^3} - \frac{(1-2v)x_1x_2}{R(R+x_3)^2}\right] \\ u_3 = \frac{P}{4\pi\mu\ cos\alpha}\left[\frac{x_1x_3}{R^3} + \frac{(1-2v)x_1}{R(R+x_3)}\right]\end{gathered} \tag{46}$$

3.4. Principle of Superposition

Until this research, no similar hybrid solution proposal has been found, which is the essence of this work. As shown, auxiliary systems are formed that can integrate the entire given system. Thus, the principle of nonlinear superposition ensures a closed form of functionally independent integrals, according to Menini and Tornambé [50], for example, linear elastic Boussinesq-Cerruti solutions, for the stress system, because it is a simple solution, considered by Nikas [51]. For the case of linear elasticity, the internal and external stress and displacement functions were:

$$\begin{gathered}\sigma_1 = \left(\frac{P}{2\pi}\left[\frac{(1-2v)}{R(R+z)} - \frac{3r^2z}{R^5}\right]\right)\Big|_{(r,\theta,z)} + \left(\frac{P(1-2v)}{2\pi}\left[\frac{x_1}{R(R+x_3)^2} - \frac{2x_1x_2^2}{R^2(R+x_3)^3} - \frac{x_1x_2^2}{R^3(R+x_3)^2}\right] - \frac{3Px_1^2}{2\pi R^5}\right)\Big|_{(x_1,x_2,x_3)} \\ \sigma_2 = \left(\frac{(1-2v)P}{2\pi}\left(\frac{z}{R^3} - \frac{1}{R(R+z)}\right)\right)\Big|_{(r,\theta,z)} + \left(\frac{P(1-2v)}{2\pi}\left[\frac{3x_1}{R(R+x_3)^2} - \frac{2x_1^3}{R^2(R+x_3)^3} - \frac{x_1}{R^3(R+x_3)^2}\right] - \frac{3Px_1x_2^2}{2\pi R^5}\right)\Big|_{(x_1,x_2,x_3)} \\ \sigma_3 = \left(-\frac{3P}{2\pi}\frac{z^3}{R^5}\right)\Big|_{(r,\theta,z)} + \left(\frac{3Px_1x_3^2}{2\pi R^5}\right)\Big|_{(x_1,x_2,x_3)}\end{gathered} \tag{47}$$

$$\begin{gathered}u_1 = \left(\frac{P}{4\mu\pi}\left[\frac{rz}{R^3} - \frac{(1-2v)r}{R(R+z)}\right]\right)\Big|_{(r,\theta,z)} + \left(\frac{P}{4\pi\mu}\left[\frac{1}{R} + \frac{x^2}{R^3} + \frac{(1-2v)}{(R+x_3)} - \frac{x^2}{R(R+x_3)^2}\right]\right)\Big|_{(x_1,x_2,x_3)} \\ u_2 = \left(\frac{P}{4\pi\mu}\left[\frac{x_1x_2}{R^3} - \frac{(1-2v)x_1x_2}{R(R+x_3)^2}\right]\right)\Big|_{(x_1,x_2,x_3)} \\ u_3 = \left(\frac{P}{4\mu\pi}\left[\frac{(2-2v)}{R} + \frac{z^2}{R^3}\right]\right)\Big|_{(r,\theta,z)} + \left(\frac{P}{4\pi\mu}\left[\frac{x_1x_3}{R^3} + \frac{(1-2v)x_1}{R(R+x_3)}\right]\right)\Big|_{(x_1,x_2,x_3)}\end{gathered} \tag{48}$$

The expressions showed a hybrid equation proposed for the stress and displacement functions, in terms of the load *P*, and considering that the hydraulic conductivity and flow conduction functions were previously described. By using the variables *r*, *t*, *h*, *z*, *x*, θ, all derivable as shown in the previous sections, so the Superposition Principle gives an individual solution as part of a general solution. The functions were defined and combined for the general solution of the HGM model, expressed in a coupled coordinate system as:

$$\begin{gathered}\rho\frac{du}{dt} = \left[\sigma_1\left(\frac{\partial u_1}{\partial(r,x_1)}\right) + \frac{\sigma_2}{r}\left(\frac{\partial u_2}{\partial(\theta,x_2)} + u_1\right) + \sigma_3\left(\frac{\partial u_3}{\partial(z,x_3)}\right)\right]_{(t)} + \\ \left[K_r\frac{\partial}{\partial r}\left(\frac{\partial h}{\partial r}\right) + \frac{K_r}{r}\frac{\partial h}{\partial r} + \frac{K_\theta}{r^2}\frac{\partial}{\partial\theta}\left(\frac{\partial h}{\partial\theta}\right) + K_z\frac{\partial}{\partial z}\left(\frac{\partial h}{\partial z}\right)\right]_{(t)} + \rho P_{(t)}\end{gathered} \tag{49}$$

This is the hybrid-coupled solution proposal of this research as a set and subset of auxiliary solutions, based on the hydrogeomechanical model presented by Teófilo-Salvador et al. [34], the present solution couple the Hydrogeological and Geomechanical processes, where the functions describe the behavior of the water flow in a soil mass. In

a transient state, the water flow approaches a radial coordinate system; upon reaching a steady state, the Cartesian component describes the surface process as runoff, thus the combination of the coordinate systems describes the hybrid part.

3.5. Case Study

The equations that make up the general solution have been tested with data obtained by Teófilo-Salvador [48], and have been graphed in Microsoft Excel 2019 as preliminary results (**Figure 3**). These graphs show the load behavior as a function of time, for intervals less than one hour, where the maximum distribution is obtained in the first fifth of the time (**Figure 3a**), consistent with the highest infiltration rate measured in the field. For the load distribution, the greatest conduction occurs on the surface, and decreases as it descends within the mass of the porous medium (**Figure 3b**). When superimposing the previous case with the effects of conduction in the medium, it is observed that the depth of the advanced profile is relatively less, the first ±15 cm can be associated with the evaporating layer, which is the boundary to prevent substantial loss of moisture to the atmosphere (**Figure 3c**). For the transient conduction, it is observed that the field points are adjusted in two-time intervals, and this is due to the fact that the measurements were for two periods of precipitation, when estimating the Root Mean Square Error (RMSE), to measure the average difference between model values and those obtained in the field, a value of 23% was obtained, which is relatively low, a good approximation using first principles of groundwater hydrology, when comparing this analytical model with Van Genuchten's empirical formulation, although a greater number of tests are needed to evaluate the reliability of the predictive model (**Figure 3d**), the first hour of measurement detects a stationary regime, and the second part as part of a feedback process, as occurs in most water flow events in soil masses, and as time increases, the absorption into deeper layers is less prominent. In **Figure 3e**, it is shown how the load distribution changes due to the change of material, being less deep for sand compared to clay. Sandy material generates bulbs with smaller radii compared to clays in a range of 10 times. Finally, **Figure 3f** shows the behavior of the energies involved due to the presence of a load (precipitation), even when the load occurred in the first hour, a variation in energies in the second, and stabilization in the third. Additionally, applying this hybrid-coupled solution proposal allows prediction at longer times, above the measurement or test times, as shown in **Figure 3f**. Hydraulic energy is positive due to the hydraulic load on the surface. Internal energy and mechanical energy balance each other over the 2-h test period. By maintaining the load constant, hydraulic and mechanical energy neutralize each other within 10 h. Between 2 and 3 h, the internal energy undergoes a transition, stabilizing at 10 h, due to the constant surface hydraulic load. This gives an answer to what really happens in soils subject to loads due to rain: they do not slide instantly, but after a certain time.

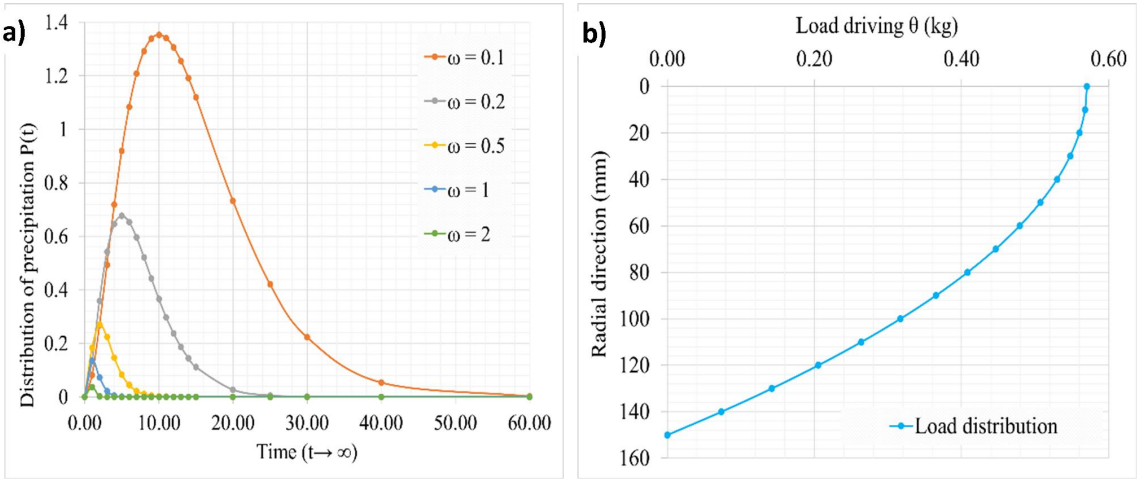

Figure 3. *Cont.*

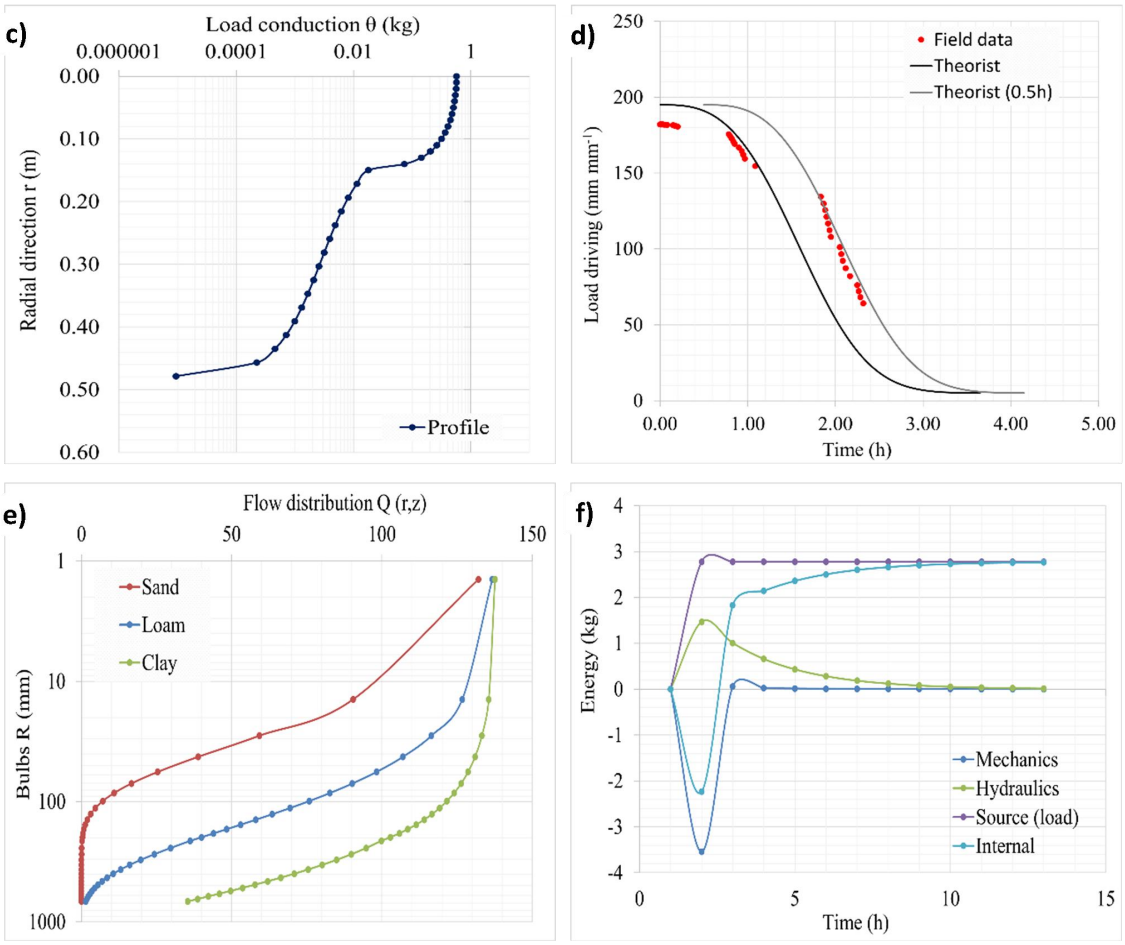

Figure 3. (**a**) Distribution of precipitation, (**b**) Load distribution at the upper limit, (**c**) Internal conduction, (**d**) Transient conduction of the internal radial, (**e**) Conduction analogous to a near-surface flow supply, (**f**) Coupled-hybrid solution of the hydrogeomechanical model.

4. Discussion

Currently, we have access to large amounts of data, but raw information is a difficult problem, so less attention has been devoted to the development of analytical, hybrid, or coupled systems, according to Thompson et al. [52]. Hybrid modeling is more reliable for analysis, design, and maintenance, although more research is required; experience from field and laboratory studies can be leveraged, indicated by Kantarji [53], but they have presented greater precision, with great advantages over empirical, classic, or conventional solutions. The soil+water system evolves through dynamic interaction, for example, the superposition and combination of the physical system includes control at the modeling level, according by Platzer [54]. As hybrid systems are more challenging than continuous dynamical systems and discrete systems, described by Platzer [55], this proposed hybrid system solution involves rigorous mathematical analysis. Due to the complexity of the system, it was difficult to find exact solutions, in accordance with Slaughter [46], but the Saint-Venant principle shows an approximate solution considering linear elasticity of the soil.

In classical approaches to dynamical systems with discontinuities, partial functions can be a solution as a piecewise continuous function of time, mentioned by Sanfelice et al. [36]. Hybrid numerical-analytical approaches are a good method, for the flow of Newtonian fluids conducted within flat channels of parallel plates subjected to a uniform, and constant external field, laminar and incompressible flow in steady state, and constant physical properties, in the context of Andrade et al. [56], as occurs in soil mass plus water flow. Currently, in hydrogeology, it is

common to resort to developed empirical formulations, such as that of Maulem-Van Genuchten, according to Wesseling et al. [57]. However, it has been demonstrated numerically and analytically that Richards' equation, together with van Genuchten's static equilibrium pressure-saturation relationships, and Mualem's hydraulic conductivity, are incompatible due to the saturation overshoot for infiltration in porous media, indicated by Xiong [42]. These traditional approaches have done little to allow new mathematical models, such as the one developed in this research, to take root.

When considering the precipitation and flow of water as a load, the forces are continuously distributed over the area of contact with the mass, and the magnitude of these forces is defined by their intensity, that is, the amount of force per unit area, described by Timoshenko and Goodier [58], and everything is a function of a single dynamic variable, *P*. If the forces act on a small portion of the surface of the elastic body (as occurs in landslides, sinkholes, etc.), they can be replaced by a system of statically equivalent forces acting on the same portion of the surface, so that the distribution of charges produces changes in local stresses in accordance with Saint Venant's principle.

The displacement depends on the intensity of the applied load and the material, and in elastic cases, it is normal to the direction of the load, and the displacement on the surface tends to disappear at the point where the load is applied, indicated by Anagnostou et al. [59]. Therefore, not all soils affected by water flow tend to move. Convective fluid flow transfer in partially porous channels with local hydraulic, or thermal imbalance generates an expansion function, typical of coupled multilayers, but gives greater precision, leading to more optimistic flow transfer predictions, since the coupled phase is solid and the porous medium is fluid, according to Lisboa et al. [60]. This precision can be achieved with rigorous programs or codes, but they have only been coded in Excel, since according to Moukalled et al. [61], it is necessary to discretize, generate the solution method (combination of multicell methods, iterative solutions or coupled finite methods), and thus the graphical visualization of the process, but it requires a greater investment of time and money.

The hybrid-coupled solution this research, is shown in equation 49 was in terms of expressions 33, 38, 40, 47, and 48, for the hydrogeomechanical (HGM) system, developed from Teófilo-Salvador et al. [34], but because the internal energy equation is a fundamental equation of mechanics, this solution could be applied to various multidisciplinary problems in other areas: Mechanics, Geomechanics, and Hydrogeology, such as soil+water problems adding infiltration forces from an analytical, experimental and laboratory context, presented by Teófilo-Salvador [62]. Such a coupled solution in heterogeneous shale volume fracturing, according to Shang et al. [63], since it involves a coupled thermohydrogeomechanical (THGM) process in fractured rocks, which involves transient fluids, conduction, convection, energy exchange, permeability evolution, and fracture stress variation, in the context of Yan et al. [64]. Disciplines in which variations in surface and internal energy occur when the body or substance is subjected to changes in temperature, or due to the presence of thermal or hydraulic flow, and that in this research analogies were made based on heat flow and fluid flow. In the short term, it will be necessary to evaluate thermal, hydraulic, mechanical, and chemical processes as coupled processes, presented by Teófilo-Salvador [65], with the solution of the partial differential equations to describe the energy or mass balance; ignoring the coupling can lead to a simplification and not adequately represent the systems, according to McDermott et al. [66].

Although this solution may still be limited for soil-water systems due to a lack of experimental and laboratory data, and because of phase changes, future work is expected to apply it to problems such as medical physics (blood flow), volcanology (magmatic flows), and materials (fresh concrete, ceramics, etc.). Currently, the formulations of the proposed solution continue to be synthesized, to encode and generate numerical simulations and field and laboratory experiments. This first physical-mathematical part allows us to contextualize reviews, suggestions, and opinions of other researchers, and thereby correct, increase, or provide feedback on the solution of the theory proposed in this research, in order to substantially improve scientific advances in today's world using hybrid or coupled solutions.

5. Conclusions

The most important contributions:

1) It is possible to couple the equations of underground fluid flow with the effects produced by mechanical stresses, deformations, and displacements, from a supply source such as precipitation from the surface, as a conceptualization of nonlinear physics.

2) Modern mechanical formulations can be adapted to geomechanical problems due to hydrogeological effects. By treating the coordinate axes, it is possible to estimate the variation of internal forces and displacements, as well as surface forces and displacements, as a function of a single variable: the hydraulic load *P*.
3) Although various measurable parameters are required, such as field, sampling, laboratory tests, cabinet adjustments, and treatment of the proposed solution, the latter offers a prediction alternative, in the case of soils subject to hydraulic loads due to precipitation, to alert on mass removal processes for longer times, than those of initial incidence of fluid flow on the porous medium and its advance to deeper layers as a function of time.
4) Internally, energy varies at different soil moisture contents: dry, saturated, and supersaturated, generating dynamic processes (landslides or collapses). Externally, in supersaturated soil, the energy is purely hydraulic, manifesting as a parallel and above-surface mobilization force, as runoff or flooding.

Funding

The research was financially supported by the SECIHTI Mexico, for postgraduate studies Master and Doctorate 2013–2019, and Postdoctoral stay 2021–2023 with numbers 930457 and 2420881, and the current authorized project 8085107.

Institutional Review Board Statement

Not applicable.

Informed Consent Statement

Not applicable.

Data Availability Statement

A raw Excel file of the source field information is included, unprocessed. However, if you require the data sets used and analyzed during this study, they are available from the corresponding author upon reasonable request.

Acknowledgments

The author thanks the Secretaría de Ciencia, Humanidades, Tecnología e Innovación from Mexico, and the National Autonomous University of Mexico for their support during the completion of academic research.

Conflicts of Interest

The author declares no conflict of interest.

AI Use Statement

The author declares that no artificial intelligence (AI) tools were used in the preparation of this manuscript.

References

1. Heemels, W.P.M.H.; Lehmann, D.; Lunze, J.; et al. Introduction to hybrid systems. In *Handbook of Hybrid Systems Control: Theory, Tools, Applications*; Jan, L., Francoise, L.-L., Eds.; Cambridge University Press: Cambridge, UK, 2009; pp. 3–30. [CrossRef]
2. Mittal, H.; Al, A.A.; Alhassan, S.M. Hybrid super-porous hydrogel composites with high water vapor adsorption capacity—Adsorption isotherm and kinetics studies. *J. Environ. Chem. Eng.* **2021**, *9*, 106611. [CrossRef]
3. Tran, K.M.; Bui, H.H.; Nguyen, G.D. Hybrid discrete-continuum approach to model hydromechanical behavior of soil during desiccation. *J. Geotech. Geoenviron. Eng.* **2021**, *147*. [CrossRef]
4. Pan, S.; Yamaguchi, Y.; Suppasri, A.; et al. MPM-FEM hybrid method for granular mass-water interaction problems. *Comput. Mech.* **2021**, *68*, 155–173. [CrossRef]
5. El-Zorkany, H.L.; Balasubramanian, R. Hybrid computer solution of PDE'S using Laplace modified Galerkin approximation. *Math. Comput. Simul.* **1981**, *23*, 304–311. [CrossRef]
6. Asaoka, A.; Nakano, M.; Noda, T. Soil-water coupled behaviour of saturated clay near/at critical state. *Soil*

Found. **1994**, *34*, 91–105. [CrossRef]
7. Lima, J.A.; Perez-Guerrero, J.S.; Cotta, R.M. Hybrid solution of the averaged Navier–Stokes equations for turbulent flow. *Comput. Mech.* **1997**, *19*, 297–307. [CrossRef]
8. Erduran, K.S. Further application of hybrid solution to another form of Boussinesq equations and comparisons. *Int. J. Numer. Methods Fluids* **2006**, *53*, 827–849. [CrossRef]
9. Huang, X.; Rudolph, D.L. A hybrid analytical-numerical technique for solving soil temperature during the freezing process. *Adv. Water Resour.* **2022**, *162*, 104163. [CrossRef]
10. Nastase, A. Hybrid numerical solutions for three-dimensional compressible Navier–Stokes layer. *Proc. Appl. Math. Mech.* **2010**, *9*, 493–494. [CrossRef]
11. Xie, M.; Navas, P.; López-Querol, S. A stabilized semi-implicit double-point material point method for soil-water coupled problems. *Comput. Part. Mech.* **2025**, *12*, 3389–3419. [CrossRef]
12. Chen, T.-M. Numerical solution of hyperbolic heat conduction problems in the cylindrical coordinate system by the hybrid Green's function method. *Int. J. Heat Mass Transf.* **2010**, *53*, 1319–1325. [CrossRef]
13. Luo, C.-l.; Yu, Y.-y.; Zhang, J.; et al. Thermal-water-salt coupling process of unsaturated saline soil under unidirectional freezing. *J. Mt. Sci.* **2023**, *20*, 557–569. [CrossRef]
14. Madureira, L.R.; Melo, F.Q. Hybrid formulation solutions for stress analysis of curved pipes with welded bending joints. *Eng. Fract. Mech.* **2010**, *77*, 2992–2999. [CrossRef]
15. Nick, H.M.; Matthäi, S.K. A hybrid finite-element finite-volume method with embedded discontinuities for solute transport in heterogeneous media. *Vadose Zone J.* **2011**, *10*, 299–312. [CrossRef]
16. Zhang, M.; Wen, Z.; Xue, K.; et al. A coupled model for liquid water, water vapor and heat transport of saturated-unsaturated soil in cold regions: Model formulation and verification. *Environ. Earth Sci.* **2016**, *75*, 701. [CrossRef]
17. Sun, J.; Sun, H.; Lu, M.; et al. Finite-difference solution for dissipation of excess pore water pressure within liquefied soil stabilized by stone columns with consideration of coupled radial-vertical seepage. *Soil Dyn. Earthq. Eng.* **2024**, *176*, 108328. [CrossRef]
18. Tu, S.; Li, W.; Zhang, C.; et al. Seepage effect on progressive failure of shield tunnel face in granular soils by coupled continuum-discrete method. *Comput. Geotech.* **2024**, *166*, 106009. [CrossRef]
19. Hai, M.; Wang, M.; Meng, S.; et al. Research on hydro-thermal coupling model of canal foundation soil based on particle grading curve predicting soil-water characteristic curve. *Case Stud. Therm. Eng.* **2024**, *56*, 104270. [CrossRef]
20. Deng, C.; Zhang, Y.; Bailey, R.T. Evaluating crop-soil-water dynamics in waterlogged areas using a coupled groundwater-agronomic model. *Environ. Model. Softw.* **2021**, *143*, 105130. [CrossRef]
21. Nguyen, T.T.; Indraratna, B. Fluidization of soil under increasing seepage flow: An energy perspective through CFD-DEM coupling. *Granular Matter* **2022**, *24*, 80. [CrossRef]
22. Sun, R.; Ma, J.; Sun, X.; et al. Responses of soil water-root coupling and coupling effects on grapevines to irrigation methods in extremely arid region. *Agric. Water Manag.* **2024**, *302*, 108984. [CrossRef]
23. Wang, B.; Wang, P.; Zhao, M.; et al. Three-dimensional fully coupled analytical solution for a water-pile-saturated soil system under vertical P-wave incident. *Appl. Math. Model.* **2025**, *138*, 115825. [CrossRef]
24. Shao, J.; Liu, L.; Cui, J.; et al. Enhancing the coupling coordination of soil-crop systems by optimizing soil properties and crop production via subsoiling. *Soil Tillage Res.* **2025**, *248*, 106438. [CrossRef]
25. Han, G.; Huo, J.; Hu, R.; et al. Coupling relationships between vegetation and soil in different vegetation types in the Ulan Buh Desert and the Kubuqi Desert. *Front. Plant Sci.* **2025**, *16*, 1505526. [CrossRef]
26. Ambati, V.R.; Bokhove, O. Space-time discontinuous Galerkin finite element method for shallow water flows. *J. Comput. Appl. Math.* **2007**, *204*, 452–462. [CrossRef]
27. Atangana, A.; Botha, J.F. Analytical solution of the groundwater flow equation obtained via homotopy decomposition method. *J. Earth Sci. Clim. Change* **2012**, *3*, 115. [CrossRef]
28. Raats, P.A.C.; Gardner, W.R. Comparison of empirical relationships between pressure head and hydraulic conductivity and some observations on radially symmetric flow. *Water Resour. Res.* **1971**, *7*, 921–928. [CrossRef]
29. López-Acosta, N.P. Numerical modeling of water flow problems. Available online: https://www.smig.org.mx/archivos/comite/6.pdf (accessed on 14 June 2025). (in Spanish)
30. Nowinski, J.L. On the three-dimensional Cerruti problem for an elastic nonlocal half-space. *Z. Angew. Math. Mech.* **1992**, *72*, 243–249. [CrossRef]
31. Marmo, F.; Sessa, S.; Rosati, L. Analytical solution of the Cerruti problem under linearly distributed horizontal loads over polygonal domains. *J. Elast.* **2016**, *124*, 27–56. [CrossRef]
32. Li, C.; Zou, J-f. Anisotropic elasto-plastic solutions for cavity expansion problem in saturated soil mass. *Soil*

Found. **2019**, *59*, 1313–1323. [CrossRef]
33. Ye, H.; Michel, A.N.; Hou, L. Stability theory for hybrid dynamical system. *IEEE Trans. Autom. Control* **1998**, *43*, 461–474. [CrossRef]
34. Teófilo-Salvador, E.; Morales-Reyes, G.P.; Muciño-Castañeda, R.; et al. Hydrogeomechanical model: Soil mass + water flow. *Concienc. Tecnol.* **2019**, *57*, 1–13. Available online: http://www.redalyc.org/articulo.oa?id=94459796007 (in Spanish)
35. Courant, R.; John, F. *Introduction to Calculus and Analysis*; John Wiley and Sons, Inc.: New York, NY, USA, 1965. Available online: https://www.astrosen.unam.mx/~aceves/Metodos/ebooks/courant_john1.pdf
36. Sanfelice, R.G.; Goebel, R.; Teel, A.R. Generalized solutions to hybrid dynamical systems. *ESAIM: COCV* **2008**, *14*, 699–724. [CrossRef]
37. Rakoto-Ravalontsalama, N. Control of hybrid systems and discrete-event systems. Available online: https://theses.hal.science/tel-01761771 (accessed on 14 June 2025).
38. Michel, A.N.; Hou, L.; Liu, D. *Stability of Dynamical Systems*; Springer Science+Business Media LLC: Boston, MA, USA, 2009. [CrossRef]
39. Teófilo-Salvador, E.; Morales Reyes, G.P.; Esteller Alberich, M.V.; et al. Parameters controlling deep percolation in a wheat crop. *Terra Latinoamericana* **2019**, *37*, 57–68.
40. Richards, L.A. Capillary conduction of liquids through porous mediums. *Physics* **1931**, *1*, 318–333. [CrossRef]
41. Richardson, L.F. *Weather Prediction by Numerical Process*; Cambridge University Press: Cambridge, UK, 1922. Available online: https://dn721509.ca.archive.org/0/items/weatherpredictio00richrich/weatherpredictio00richrich.pdf
42. Xiong, Y. Flow of water in porous media with saturation overshoot: A review. *J. Hydrol.* **2014**, *510*, 353–362. [CrossRef]
43. Philip, J.R. Steady infiltration from buried point sources and spherical cavities. *Water Resour. Res.* **1968**, *4*, 1039–1047. [CrossRef]
44. Carslaw, H.S.; Jaeger, J.C. *Conduction of Heat in Solids*; Oxford University Press: Oxford, UK, 1959. Available online: https://archive.org/details/conductionheatin0000hsca/page/n9/mode/2up
45. Unsworth, J.; Duarte, F.J. Heat diffusion in a solid sphere and Fourier theory: An elementary practical example. *Am. J. Phys.* **1979**, *47*, 981–983. [CrossRef]
46. Slaughter, W.S. *The Linearized Theory of Elasticity*; Springer Science+Business Media LLC: New York, NY, USA, 2002. [CrossRef]
47. Sadd, M.H. *Elasticity: Theory, Applications, and Numerics*; Elsevier: Burlington, MA, USA, 2014.
48. Teófilo-Salvador, E. Hydrogeomechanical Model to Evaluate Soil Slippage Due to Subsurface Water Flow. PhD Thesis, Universidad Autónoma del Estado de México, Toluca, México, 2019. (in Spanish)
49. van Genuchten, M.T. A closed-form equation for predicting the hydraulic conductivity of unsaturated soils. *Soil Sci. Soc. Am. J.* **1980**, *44*, 892–898. Available online: https://www.ars.usda.gov/arsuserfiles/20360500/pdf_pubs/p0682.pdf
50. Menini, L.; Tornambé, A. Nonlinear superposition formulas: Some physically motivated examples. In Proceedings of the 2011 50th IEEE Conference on Decision and Control and European Control Conference, Orlando, FL, USA, 12–15 December 2011; pp. 1092–1097. [CrossRef]
51. Nikas, G.K. Boussinesq-Cerruti functions and a simple technique for substantial acceleration of subsurface stress computations in elastic half-spaces. *J. Eng. Tribol.* **2006**, *220*, 19–28. [CrossRef]
52. Thompson, J.A.; Brodzik, M.J.; Silverstein, K.A.T.; et al. EASE-DGGS: A hybrid discrete global grid system for earth sciences. *Big Earth Data* **2022**, *6*, 340–357. [CrossRef]
53. Kantarji, I.G. Hybrid modeling of wave processes in the scientific justification of hydraulic solutions. *IOP Conf. Ser.: Mater. Sci. Eng.* **2020**, *905*, 012035. [CrossRef]
54. Platzer, A. *Logical Analysis of Hybrid Systems*; Springer-Verlag: Berlin, Germany, 2010. [CrossRef]
55. Platzer, A. The complete proof theory of hybrid systems. In Proceedings of the 2012 27th Annual ACM/IEEE Symposium on Logic in Computer Science, New Orleans, LA, USA, 25–28 June 2012. [CrossRef]
56. Andrade, P.F.; Negrão, M.E.; da Silva, B.C.; et al. Hybrid solutions obtained via integral transforms for magnetohydrodynamic flow with heat transfer in parallel-plate channels. *Int. J. Numer. Methods Heat Fluid Flow* **2018**, *28*, 1474–1505. [CrossRef]
57. Wesseling, J.G.; Ritsema, C.J.; Stolte, J.; et al. Describing the soil physical characteristics of soil samples with cubical splines. *Transp. Porous Media* **2008**, *71*, 289–309. [CrossRef]
58. Timoshenko, S.; Goodier, J.N. *Theory of Elasticity*; McGraw-Hill Book Company, Inc.: New York, NY, USA, 1951.
59. Anagnostou, D.S.; Gourgiotis, P.A.; Georgiadis, H.G. The Cerruti problem in dipolar gradient elasticity. *Math.*

Mech. Solids **2015**, *20*, 1088–1106. [CrossRef]
60. Lisboa, K.M.; Zanon, Z.J.L.; Machado, C.R. Hybrid solutions for thermally developing flows in channels partially filled with porous media. *Numer. Heat Transf. B Fundam.* **2021**, *79*, 189–215. [CrossRef]
61. Moukalled, F.; Mangali, L.; Darwish, M. *The Finite Volume Method in Computational Fluid Dynamics: An Advanced Introduction with OpenFOAM and Matlab*; Springer: Cham, Switzerland, 2016. [CrossRef]
62. Teófilo-Salvador, E. Model of water flow infiltration force in a soil mass. *Terra Latinoamericana* **2025**, *42*, 1–13.
63. Shang, X.; Zhang, Z.; Yang, W.; et al. A thermal-hydraulic-gas-mechanical coupling model on permeability enhancement in heterogeneous shale volume fracturing. *Mathematics* **2022**, *10*, 3473. [CrossRef]
64. Yan, X.; Xue, K.; Liu, X.; et al. A novel numerical method for geothermal reservoirs embedded with fracture networks and parameter optimization for power generation. *Sustainability* **2023**, *15*, 9744. [CrossRef]
65. Teófilo-Salvador, E. Computational review for fluid flow—Heat transfer in stress deformation in porous/fractured media, THGMC. *Earth Planet. Sci.* **2025**, *4*, 89–108. [CrossRef]
66. McDermott, C.; Bond, A.; Fraser, H.A.; et al. Application of hybrid numerical and analytical solutions for the simulation of coupled thermal, hydraulic, mechanical and chemical processes during fluid flow through a fractured rock. *Environ. Earth Sci.* **2015**, *74*, 7837–7854. [CrossRef]